

## **HIGHLY LUMINESCENT MoS<sub>2</sub> NANOSHEETS OBTAINED VIA TOP-DOWN APPROACH**

**Nitesh Dogra, Mandeep Singh and Sandeep Sharma\***

Department of Physics,

Guru Nanak Dev University, Amritsar, Punjab India.

\*E-mail : [sandeepscl@gmail.com](mailto:sandeepscl@gmail.com)

### **ABSTRACT**

Here, we report the synthesis of hetero-dimensional nanosheets of MoS<sub>2</sub> via a facile probe-sonication method. Structural analysis using X-ray diffraction revealed the hexagonal phase of synthesized MoS<sub>2</sub> nanosheets. Transmission electron microscopy images indicated the presence of (004) planes and hexagonal symmetry of the processed nanosheets. These results were further supported by Raman spectra, which clearly revealed the reduction in intensity ratio of A<sub>1g</sub> and E<sub>2g</sub><sup>1</sup> modes of MoS<sub>2</sub>. Whereas, MoS<sub>2</sub> in bulk form is an indirect bandgap material and no emission is expected, the scaled MoS<sub>2</sub> nanosheets have shown significant photoluminescence emission in the wavelength range from 300 to 550 nm. These results suggest that an indirect to direct bandgap transformation in MoS<sub>2</sub> with reduction in no of layers give rise to enhancement in the photoluminescence emission. This way one can optimize the emission in desired range of the spectrum.

**Keywords:** MoS<sub>2</sub>, Photoluminescence, Exciton.

---

### **INTRODUCTION**

In the last decade, significant developments have taken place in the area of material science. Specially talking about two-dimensional materials, like graphene, due to its superior properties, such as very large electronic mobility and surface-area to volume ratio has been extensively studied for applications in electronic and gas sensing purpose (Geim 2007). However, absence of bandgap makes it unsuitable for many digital electronic based applications. Though, bandgap can be introduced in graphene via processing induced modifications in graphenenanosheets, but it unnecessary complicates the synthesis route and is discouraged (Matthew 2010, Choi 2010). Transition metal dichalcogenides (TMDCs)

such as MoS<sub>2</sub>, WS<sub>2</sub> and TiS<sub>2</sub>, on the other hand in bulk form possess an intrinsic indirect bandgap which change into a direct bandgap in monolayer form (Kuc 2011, Pandey 2016). Due to an indirect bandgap, the photoluminescence is feeble and cannot be detected (Sharm 2017). On the other hand, in scaled nanosheets, various recent investigations have claimed strong photoluminescence in TMDCs nanosheets (Splendiani 2010). This was attributed to the transformation from an indirect bandgap material to a direct bandgap material. As revealed by recent theoretical simulations, this transformation is accompanied with changes in electronic properties of the material that further depend on number of layers (Kuc 2011). The modified electronic properties and

their connection with the number of layers offer an opportunity to explore their physical properties from various applications point of view. Main concern behind the exploration of nanoscaled materials is the fascinating physical properties and secondly a wide range of applications they possess in their scaled form, thus providing thrust to push their size to nano-regime.

Recently, various techniques have been used to obtain materials in nanostructured form. Among these, top-down approach offers a quick and facile method (Sharma 2017). Here, we report such a method to obtain MoS<sub>2</sub> nanosheets via liquid-based exfoliation using probe sonication approach. We report the synthesis of MoS<sub>2</sub> nanosheets in de-ionized (DI) water. Structural analysis has indicated their successful synthesis and later optical characterization revealed the presence of strong photoluminescence emission in the wavelength range from 300 nm to 550 nm.

## MATERIAL AND METHODS

The crystalline MoS<sub>2</sub> powder was purchased from Sigma Aldrich India. For sample preparation, 2 g of MoS<sub>2</sub> was mixed with 50 ml of de-ionized (DI) water. This mixture was then processed using high energy Probe Sonicator (750 Watt, 20 kHz, PCI-Analytics, India) for 2 hours. After probe sonication, the dispersion of MoS<sub>2</sub> in water along with floating MoS<sub>2</sub> thin sheets was obtained. The floating nanosheets were transferred onto glass slide using dip coating method and the sample so obtained was named A1. The dispersion was then centrifuged at 12,000 rpm for 20 minutes. After centrifugation, a yellow coloured dispersion was obtained. Another sample on a clean glass slide was prepared from this dispersion using drop casting method. This sample was dried in a vacuum oven at 60<sup>o</sup> C and was named B1.

X-ray diffraction patterns of different samples were recorded using Shimadzu 7000 X-ray diffractometer using Cu K $\alpha$  radiation source

( $\lambda = 1.5406 \text{ \AA}$ ). The Raman spectra were obtained using RenishawInVia Micro Raman spectrometer with 488 nm excitation at room-temperature. Morphology and crystal structure of the sample B1 was investigated using JEOL JEM-2100 high-resolution transmission electron microscopy (HR-TEM). The absorption spectra were measured using Shimadzu UV-3600 spectrophotometer. The Photoluminescence (PL) spectra of the sample B1 were recorded using Perkin Elmer LS-55 fluorescence spectrometer.

## RESULTS AND DISCUSSION

Fig.1 shows the X -rays diffractogram for sample A1 and B1. All the peaks corresponding to various planes matches well with the JCPDS card 77-1716 of MoS<sub>2</sub>. In sample A1 the relative peak intensity of the peaks other than (002) is reduced. Relatively sharp (002) peak indicates the dominant exposure of basal plane in layered MoS<sub>2</sub>. The inset in (b) shows the enhanced view of peaks other than (002). Sample B1 displays only three peaks where (002) peak shows relatively lower intensity and is slightly broadened. This indicates that not only the sample thickness but lateral dimensions of the MoS<sub>2</sub> crystallites have also reduced. Fig. 2 displays transmission electron microscopic images of MoS<sub>2</sub> nanosheets at different resolutions. In panel a, one can clearly see the nanosheets with lateral dimensions ranging from a few nm to hundreds of nm. Colour contrast indicates the variable thickness of the obtained nanosheets which have been obtained after probe sonication. Panel b represents HRTEM image of the nanosheets and clearly shows fringes with interplanar spacing of 3.1  $\text{\AA}$  corresponding to (004) planes of MoS<sub>2</sub>. The lower inset in the same image represents the magnified view of highlighted region. The hexagonal symmetry of MoS<sub>2</sub> is clearly visible from the inset. Panel c represents the digitally filtered image of the part of Figure b. The hexagonal symmetry along with parallel

running planes with interplanar spacing of 0.31 nm belong to MoS<sub>2</sub>.

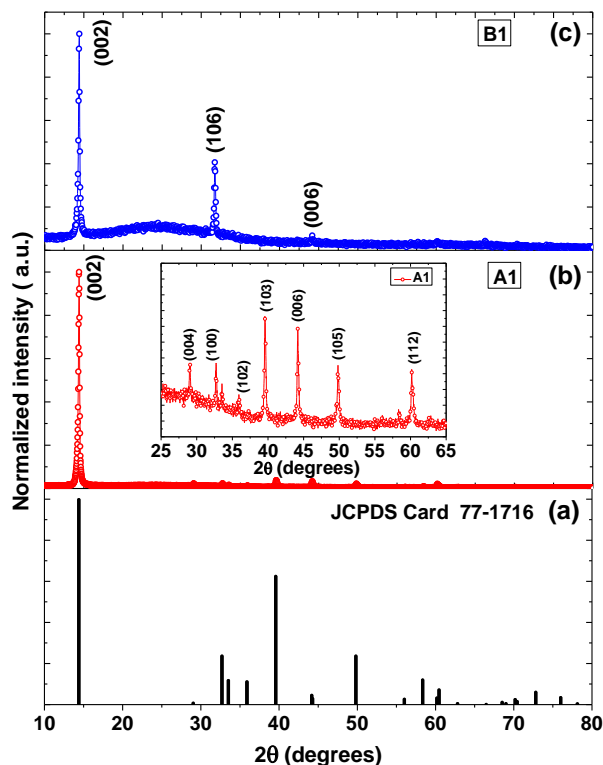


**Figure 1. X-ray diffractogram from probe-sonicated (b) thin sheets and (c) suspension of MoS<sub>2</sub> and (a) standard JCPDS data shown for the sake of comparison.**

Raman spectroscopy was further used for determining the vibrational properties of the synthesized MoS<sub>2</sub> nanosheets. Raman spectroscopy offers a non-destructive method for identification of the materials, and determination of their structural properties and various phases in which they exist. Figure 3 compares the Raman spectra obtained from bulk crystalline powder, and samples A1 and B1. Here, only two first-order Raman active modes, A<sub>1g</sub> and E<sub>2g</sub><sup>1</sup> have been shown. Figure on the right displays the relative motion of different atoms in these modes. The mode A<sub>1g</sub> arises due to out-of-plane motion of the two sulfur atoms while transition metal atom stays fixed. On the other hand, the mode E<sub>2g</sub><sup>1</sup> originates due to relative in-plane motion of the sulfur and molybdenum atom. Note that in

the latter case, the sulfur atoms move in one direction whereas molybdenum atoms move out-of-phase w.r.t. sulfur atoms. As expected, the separation between these two modes decreases with decreasing thickness of the material and this separation also serves as an excellent indicator for the number of layers in MoS<sub>2</sub>. Surprisingly, in sample A1, this separation has reduced but in B1 it increases further. This might arise due to dimensional scaling along vertical as well as lateral direction. Another important parameter that indicates scaling of the starting bulk material is the intensity ratio of A<sub>1g</sub> and E<sub>2g</sub><sup>1</sup> modes given in last row of Table 1.

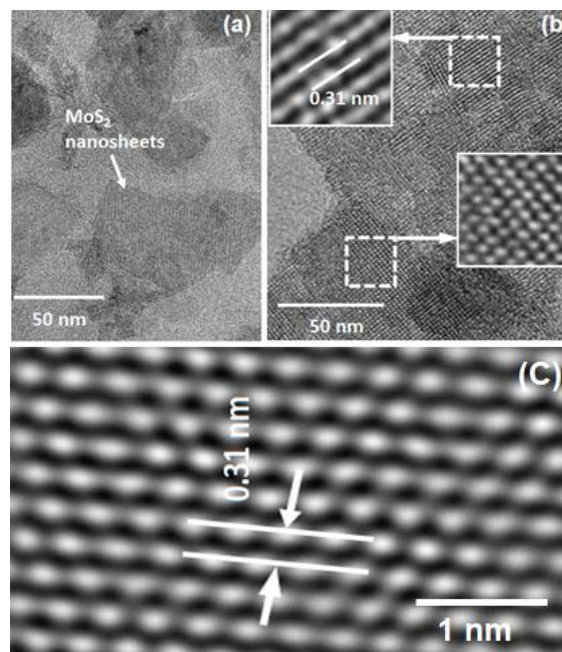


**Figure 2. (a) Low resolution transmission electron microscopic image of MoS<sub>2</sub> nanosheets displaying variable colour contrast (b) HRTEM image of the nanosheets showing fringes and (c) digitally filtered image of MoS<sub>2</sub> nanosheets displaying hexagonal symmetry of the MoS<sub>2</sub>.**

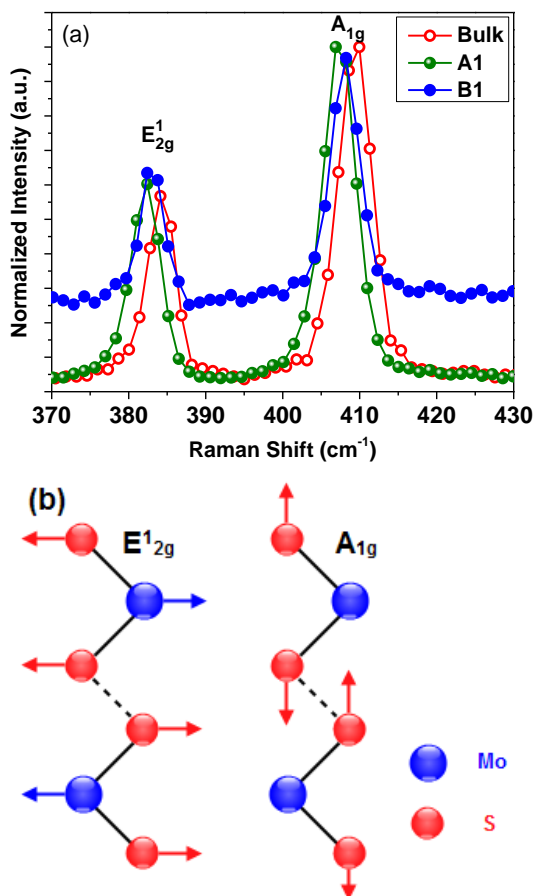


**Figure 3.** Comparison between Raman spectra obtained from bulk crystalline powder, thin nanosheets (A1) and dispersion (B1) of MoS<sub>2</sub> with an excitation wavelength of 488 nm. (b) Vibrations of transition metal and chalcogen atoms in E<sup>1</sup><sub>2g</sub> and A<sub>1g</sub> modes.

This ratio decrease from 1.77 (bulk) to 1.66 (A1) to 1.52 (B1), thus clearly suggesting that dimensional scaling has taken place vertically as well as laterally. The E<sup>1</sup><sub>2g</sub> and A<sub>1g</sub> modes exhibit opposite trends when sample changes from bulk MoS<sub>2</sub> to 1L-MoS<sub>2</sub>. Therefore, separation between these two modes and their intensity ratio serves as an important tool to identify the number of layers (vertical scaling) with atomic-level precision and lateral scaling of the dimensions of crystallites (Zhang 2015). For these two modes, the linear chain model predicts (only van der Waals interactions included) a decrease in frequency

with decrease in number of layers (Zhang 2013).

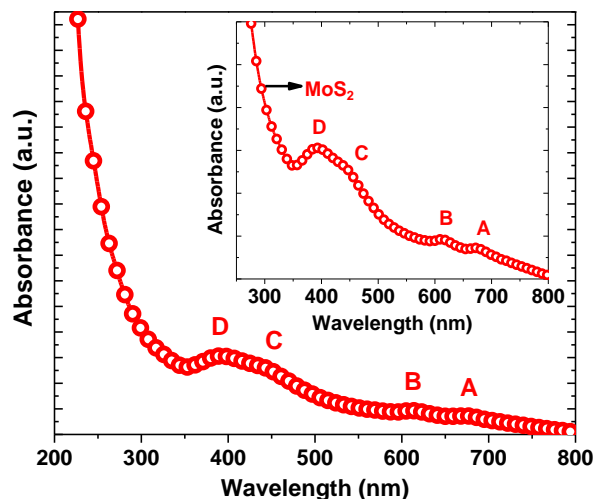


**Figure 4.** Absorption spectra from MoS<sub>2</sub> nanosheets.

Contrary to this, these two modes have shown an opposite trends with decreasing thickness from bulk to monolayer (Lee 2010). This trend of frequency dependence of these two modes indicates that interactions other than weak van der Waals forces do exist and need to be considered (Lee 2010, Molina 2011, Luo 2013). On the other side, Raman spectra from MoS<sub>2</sub> or WS<sub>2</sub> based nanostructures have revealed totally different trends of frequency dependence of these two modes (Sharma 2017, Mukherjee 2015, Gopalkrishnan 2014). For instance, Sharma et al. (Sharma 2017) have shown a blue-shift in these two modes for WS<sub>2</sub> nanostructures. In case of MoS<sub>2</sub> nanostructures Mukherjee et al. (Mukherjee 2015) have shown similar blue shift whereas Gopalkrishnan et al. have shown red-shift in these two first-order Raman modes w.r.t bulk MoS<sub>2</sub> (Gopalkrishnan 2014). Though, in monolayer MoS<sub>2</sub> or similar TMDCs, the anomalous blue shift in E<sup>1</sup><sub>2g</sub> mode with decreasing thickness has been understood by invoking surface effects (Luo 2013) on Raman frequencies, similar investigations on scaled nanostructures of TMDCs are lacking. These anomalous observations in scaled

nanostructures reflects the presence of other interactions like stacking induced structural changes or defects and behaviour of coulomb interactions (Lee 2010, Molina 2011). However, the exact understanding has still remained elusive (Bonaccorso 2013) and further theoretical investigations are needed.

**Table 1. Raman shift for  $E_{2g}^1$  and  $A_{1g}$  modes and corresponding intensity ratio ( $A_{1g}/E_{2g}^1$ )**

Sample	$E_{2g}^1$	$A_{1g}$	Intensity( $A_{1g}/E_{2g}^1$ )
Bulk	384.12	409.95	1.77
A1	382.43	406.9	1.66
B1	382.41	408.24	1.52

**Table 2. List of various photoluminescence peaks obtained from  $MoS_2$  based dispersion.**

Excitation wavelength ( $\lambda_{exc}$ in nm)	Photoluminescence emission peaks (in nm)
250	346, 387, 438
275	346, 407, 462
290	346, 403, 440
300	346, 404, 445
310	352, 402, 440
320	364, 388, 417, 450
330	373, 394, 424, 461, 526
340	386, 404, 430, 462, 513

**UV-Visible spectra**

Further, to gain an insight about optical properties of heterodimensional  $MoS_2$  nanosheets, optical absorption spectra from suspension were measured. Fig. 4 shows the UV-visible absorption spectra of  $MoS_2$  suspension in DI-water. Four characteristics peaks marked as A (670 nm), B (610 nm), C (450 nm), and D (390 nm) appear in the spectra. Peaks A and B are characteristics excitonic peaks arising from transitions between the spin-orbit coupling (SOC)

induced splitting of the states at valence band maxima and conduction band minima at k-point of the Brillouin zone.

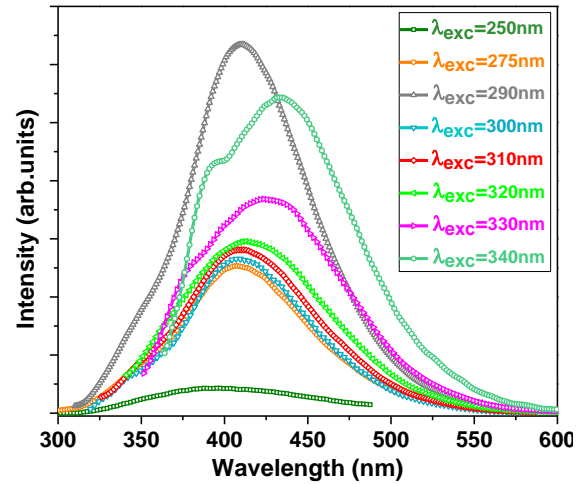


**Figure 5. Photoluminescence spectra from  $MoS_2$  nanosheets at different excitation wavelengths.**

The separation between these two peaks gives an approximate strength of the SOC strength and it matches with previously reported values (Mukherjee 2015, Boker 2001, Zhu 2011, Trainer 2017). The other two peaks marked as C and D result from transitions from the depth of valence band (Boker 2001). In addition to these four features a band edge transition occurs at  $\approx 280$  nm (4.44 eV). The direct band gap in monolayer  $MoS_2$  is around 1.89 eV, much smaller than the absorption noticed at high energy side (4.44 eV) for scaled  $MoS_2$  nanostructures. Therefore, this feature cannot be associated with the  $MoS_2$  monolayer; rather, it might arise from scaled  $MoS_2$  nanostructures. But now the question is whether dimensional scaling can give rise to such a large change in band gap or not. Historically, the increase in bandgap has been attributed to the phenomena of quantum confinement in scaled nanostructure [19,20]. The onset of quantum confinement effect can be gauged from Bohr’s radius ‘R’ for a material. The Bohr’s radius is given by:

$$R = \varepsilon \left( \frac{m_0}{\mu} \right) a_0$$

Where,  $\varepsilon$  is the dielectric constant of the material in bulk form,  $m_0$  is free electron mass and  $\mu$  being the reduced mass of electron-hole pair given by equation:  $\mu=(m_e m_h / m_e + m_h)$  and  $a_0=0.53\text{\AA}$ . Here,  $m_e$  and  $m_h$  represent the effective masses for electron and hole, respectively. For  $\text{MoS}_2$ , the dielectric constant  $\varepsilon \approx 11$  in bulk form and effective masses  $m_e=0.48m_0$ ,  $m_h=0.41m_0$ (Mukherjee 2015), giving  $\mu=0.22m_0$ . After plugging these numbers in Eqn.1, the exciton Bohr's radius for  $\text{MoS}_2$  comes out to be 2.65 nm. Hence, quantum confinement effects in  $\text{MoS}_2$  are expected when particle size is roughly below 5 nm.

The observed blue-shift of the first absorption peak in the scaled  $\text{MoS}_2$  nanostructures (or precisely quantum dots) may be qualitatively understood in terms of quantum confinement models. Under this effective mass approximation theory, the bandgap variation with particle size is governed by the equation (Wilcoxon 1995, Gan 2015):

$$E^* = E_g + \frac{h^2}{8\mu r^2} - \frac{1.8e^2}{4\pi r \varepsilon_0 \varepsilon_r} \quad (2)$$

Where,  $E_g$ ,  $\mu$ , and  $r$  represents the bandgap of bulk material, reduced mass of exciton, radius of the nanoparticle or quantum dots respectively. Here,  $\varepsilon_0$  is the permittivity of free space and  $\varepsilon_r$  is relative permittivity of the material. It should be noted that above equation is simply a first approximation and has been developed assuming the particles to be a spherical, not true in present case of layered 2-D material, however, one can acquire a qualitative idea. Further, this equation also assumes that motion of electrons and holes can be described in terms of their effective masses as mentioned above. Various effects such as effect of surface atoms, crystal anisotropy and influence of spin-orbit coupling need to be included for more sophisticated calculations. The basic approximation in Eqn.2 includes two terms: (i) the confinement energy which varies as  $1/r^2$  and (ii) electrostatic

Coulomb attraction term varying as  $1/r$ . The second term, i.e., confinement energy is always a positive term and dominates, resulting in a blue-shift in the bandgap. On the other hand, for an electron-hole pair system, the Coulomb interaction is always attractive (negative) and therefore lowers the energy of its formation. The  $1/r^2$  dependence of confinement energy makes it a dominant term and effect becomes pronounced for very small quantum dot sizes.

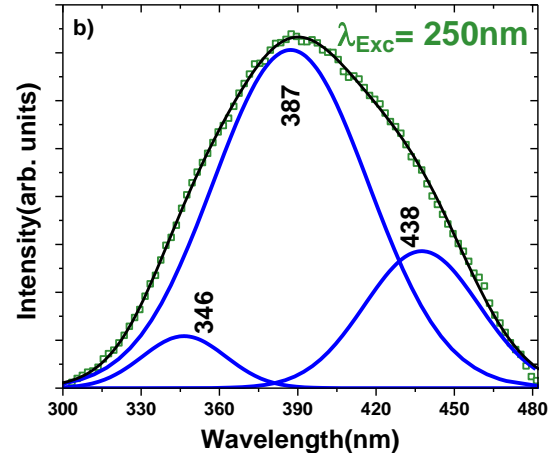


**Figure 6. De-convoluted emission spectra obtained from  $\text{MoS}_2$  nanosheets an excitation wavelength of 250 nm.**

### Photoluminescence emission spectra

In bulk form,  $\text{MoS}_2$  behaves like an indirect bandgap material and no photoluminescence emission is expected. However, after dimensional scaling of thick layered  $\text{MoS}_2$ , clear PL emission has been observed between 300-500 nm. Figure 5 displays the photoluminescence emission spectra of  $\text{MoS}_2$  suspension at different excitation wavelengths. One of the emission spectra acquired with  $\lambda_{exc} = 250$  nm is shown in Fig.6. The data was deconvoluted using Gaussian fitting function. After deconvolution three emission peaks at 346, 387 and 438 nm are obtained. A feeble emission at wavelengths higher than absorption edge is observed. The emission peaks at 387 and 438 nm coincide with 'D' and 'C' type absorptions arising from radiative recombination of electrons and holes in the

conduction and valence bands. Note that these emission are slightly shifted towards higher wavelengths. The emission peak at 346 nm is red-shifted w.r.t the absorption edge and might arise from scaled MoS<sub>2</sub> quantum dots. Following excitation of the direct transition, subsequent phonon interactions in the conduction band may cause rapid relaxation of the electrons to the conduction band minima and of the hole to the top of the valence band. This, followed by subsequent trap emission may lead to a red-shifted emission peak [21]. Note that similar fitting procedure was adopted for the emission spectra acquired at different excitation wavelengths. Various emission peaks are listed in Table.2. As we see, the emission peak at 346 nm is present even at higher excitation wavelength. Table also reveals various peaks other than observed in the absorption spectra of same sample. This together with slight red-shift in the various emission peaks could arise from slight polydispersity of the MoS<sub>2</sub> nanostructures. The variable size nanostructures possess variable bandgap and give rise to excitation dependent emission (Sharma 2017). Another, possibility could arise from the presence of several trap states as observed earlier for graphene quantum dots and for MoS<sub>2</sub> also (Chikan 2002). Further, we also notice that emission intensity increases with increase in excitation wavelength. The maximum PL emission is obtained with  $\lambda_{exc} = 290$  nm. This might be due to resonance absorption in MoS<sub>2</sub> nanostructures. As pointed earlier, the absorption from same sample displayed band edge absorption close to 300 nm. With further increase in the excitation wavelength the emission intensity reduces.

## CONCLUSIONS

In summary, we have demonstrated a facile approach to prepare highly luminescent nanosheets of MoS<sub>2</sub> via probe sonication method. Their structural analysis revealed their oriented structure towards the basal plane.

HRTEM images further confirmed the hexagonal symmetry of MoS<sub>2</sub>. Further, Raman spectroscopy analysis from different samples indicated the presence of first order Raman active modes, A<sub>1g</sub> and E<sub>2g</sub><sup>1</sup>. Their relative intensity ratio (A<sub>1g</sub>/ E<sub>2g</sub><sup>1</sup>) was found to decrease from 1.77 to 1.52 for bulk and MoS<sub>2</sub>nanosheets, implying significant reduction in thickness of the layered MoS<sub>2</sub>. Optical measurements indicated the presence of various excitonic absorptions and other direct band-to-band absorptions. Accompanied PL spectra from same sample gave emission peaks that were slightly red-shifted w.r.t absorption spectra, thus indicated the presence of traps in the processed sample.

## ACKNOWLEDGEMENTS

This work was financially supported by Department of Science and Technology, New Delhi India under research grant number EMR/2016-007483.

## REFERENCES

- Boker,T. 2001. Band structure of MoS<sub>2</sub>, MoSe<sub>2</sub>, and a-MoTe<sub>2</sub>: Angle-resolved photoelectron spectroscopy and ab-initio calculations.Phys. Rev. B,64: 235305.
- Bonaccorso, F.2013. Multiwall Nanotubes, Multilayers, and Hybrid Nanostructures: New Frontiers for Technology and Raman Spectroscopy. ACS Nano,7, 1838.
- Chikan, V. 2002.Size-dependent spectroscopy of MoS<sub>2</sub> nanoclusters. J. Phys. Chem. B,106:3794–3804.
- Choi, W. 2010. Synthesis of graphene and its applications: a review. Crit Rev Solid State Mater Sci, 35:52–71.
- Gan, Z.X. 2015. Quantum confinement effects across two-dimensional planes in MoS<sub>2</sub>quantum dots. Appl. Phys. Lett,106: 233113.
- Geim, A.K.2007. The rise of graphene. Nat Mater,6:183–191.

- Gopalkrishnan, D. 2014. MoS<sub>2</sub> quantum dot-interspersed exfoliated MoS<sub>2</sub> nanosheets, ACS Nano,5: 5297-5303.
- Kuc, A. 2011. Influence of quantum confinement on the electronic structure of the transition metal sulphide. Phys Rev B,83:245213.
- Lee, C.2010. Anomalous Lattice Vibrations of Single and Few-Layer MoS<sub>2</sub>. ACS Nano,4 (5): 2695-2700.
- Luo, X.2013. Anomalous frequency trends in MoS<sub>2</sub> thin films attributed to surface effects, Phys. Rev. B: Condens. Matter Mater. Phys.,88: 075320.
- Matthew, J. A.2010. Honeycomb carbon: a review of graphene. Chem Rev,110:132–145.
- Molina-Sanchez, A.2011. Phonons in single-layer and few-layer MoS<sub>2</sub> and WS<sub>2</sub>, Phys. Rev. B: Condens. Matter Mater. Phys., 84 155413.
- Mukherjee, S.2015.Tunable Direct Bandgap Optical Transitions in MoS<sub>2</sub> Nanocrystals for Photonic Devices. ACS Photonics,2 760–768.
- Pandey, K. 2016. First step to investigate nature of electronic states and transport in flower-like MoS<sub>2</sub>: combining experimental studies with computational calculations. Sci Rep,6:32690.
- Sharma, S.2017.Excitation-dependent photoluminescence from WS<sub>2</sub> nanostructures synthesized via top-down approach. Journal of Materials Science, 52, 11326–11336.
- Splendiani, A.2010.Emerging photoluminescence in monolayer MoS<sub>2</sub>. Nano Lett, 10:1271–1275.
- Trainer, D.J.2017. Inter-Layer Coupling Induced Valence Band Edge Shift in Mono- to Few-Layer MoS<sub>2</sub>. Scientific Reports,7: 40559.
- Wilcoxon, J.P. 1995. Strong quantum-size effects in a layered semiconductor: MoS<sub>2</sub> nanoclusters. Phys Rev B,51: 7299.
- Zhang, X.2015. Phonon and Raman scattering of two-dimensional transition metal dichalcogenides from monolayer, multilayer to bulk material. Chem Soc Rev,44:2757-2785.
- Zhang, X.2013. Raman spectroscopy of shear and layer breathing modes in multilayer MoS<sub>2</sub>. Phys. Rev B,87 115413.
- Zhu ZY (2011) Giant spin-orbit-induced spin splitting in two-dimensional transition-metal dichalcogenide semiconductors. Phys Rev B,84: 153402.